# A comparative theoretical study on the interaction of pure and carbon atom substituted boron nitride fullerenes with ifosfamide drug

Alireza Soltani [a], Elham Tazikeh-Lemeski [b],[*], Masoud Bezi Javan [c]

[a] Golestan Rheumatology Research Center, Golestan University of Medical Science, Gorgan, Iran
[b] Department of Chemistry, Gorgan Branch, Islamic Azad University, Gorgan, Iran
[c] Department of Physics, Faculty of Sciences, Golestan University, Gorgan, Iran

## ARTICLE INFO

## ABSTRACT

Anticancer drug delivery is now becoming an important scientific challenge as it allows localizing drug release near the tumor cell and avoiding secondary side effects. Based on the density functional theory (DFT) calculations, the adsorption of Ifosfamide (IFO) on a series of pure $B_{12}N_{12}$ and carbon-doped boron nitride, including $B_{12}N_6C_6$ and $B_6N_6C_{12}$ fullerenes, was carried out both in vacuum and solvent (water) environment conditions by means of PBE-1 and M06-2X functionals and 6-311 + G (d,p) basis set. The most stable chemisorption state for the IFO was through phosphoryl group ($-1.21$ eV) onto the $B_{12}N_{12}$ in comparison with chloroalkyl ($-0.35$ eV) and nitrogen atom of oxazaphosphorine ring ($-1.14$ eV) groups. To compare both environments, the computed results indicate that the adsorption of IFO in the solvent environment is more stable on the $B_{12}N_{12}$ ($-1.27$ eV), $B_{12}N_6C_6$ ($-1.86$ eV), and $B_6N_6C_{12}$ ($-1.99$ eV) fullerenes than in the vacuum environment. Our computational simulations represent that the amount of IFO loading is higher for the fullerenes, on the other hand, the interaction energy of IFO with $B_6N_6C_{12}$ is greater, which can reduce its release rate.

© 2019 Elsevier B.V. All rights reserved.

## 1. Introduction

By the first announcement of the synthesis of boron nitride ($B_{12}N_{12}$) fullerene using an arc-melting method and its detection by laser desorption time-of-flight mass spectrometry, it soon became a famous subject of many studies, especially by theoretical scientists [1]. It is an isoelectronic counterpart to the carbon-based fullerene being considered as a promising material. This fullerene gained a great attention because of its exceptional properties such as high temperature and oxidation stability, low dielectric constant, high thermal conductivity, direct band gaps affording optical and optoelectronic properties and rendering its semiconductor behavior in comparison to that of carbon based fullerenes [2–12]. Concerning the structural stability, $B_{12}N_{12}$ consisting of six tetragon rings and eight hexagon rings is considered as the most stable fullerene among its counterparts [13–16]. In previous reports, the interaction of caffeine and nicotine [17], cysteine [18], adenine, uracil and cytosine [19], 5-aminolevulinic [20] acid, 5-fluorouracil [21], phenol molecule [22], pyrimidine nucleotide [23], metformin [24], $H_2S$ gas [25], hydrogen halides [26], and aspirin [27] with the $B_{12}N_{12}$ fullerene and its derivatives have been performed using computational approaches. These evidences demonstrate that this nanocage cluster has a good ability to form a bound with biological molecules, which makes it a promising material for biomedical applications like bio-sensing, bio-imaging, and the delivery of biological and drug molecules.

3-(2-Chloroethyl)-2-[(2-chloroethyl)amino]tetrahydro-2H-1,3,2-oxazaphosphorine-2-oxide is known as an IFO drug playing an important role in cancer treatment through a combination of chemotherapy with other anticancer drugs [28,29]. IFO drug comprises a six-membered ring having three saturated carbon, oxygen, nitrogen, and phosphorus atoms, which are substituted with two chloroalkyl functional groups characterised by a single-crystal X-ray diffraction instrument [30]. So far, it has been used for the treatment of sarcomas, lymphoma, gynecologic, and testicular cancers [31]. However, it has some toxic effects upon high dosage usage that may cause central nervous system toxicity and severe nephrotoxicity in the form of Fanconi syndrome through the treatment of cancer patients [32,33]. Therefore, the determination, sensing, and delivery of this drug are of great importance. For example, Duverger et al. reported the interaction between BN nanotubes and anticancer molecules. They showed that the most stable physisorption states happened when the molecules were encapsulated inside the BN nanotube in a parallel configuration and the molecular chemisorption was possible only when the azomethine was presented above two adjacent B and N atoms of a hexagon [34]. Khalifi et al. demonstrated theoretical use of boron nitride nanotubes as a perfect container for anticancer IFO molecule [35].

This study is based on our previous experiences on the interaction of different drug and biological molecules with the nanostructures

* Corresponding author.
  *E-mail address:* elham.tazikeh@gmail.com (E. Tazikeh-Lemeski).

consisting of B and N atoms, especially the $B_{12}N_{12}$ fullerene. Accordingly, a comprehensive examination is presented here on the interaction of IFO drug molecule with the $B_{12}N_{12}$ fullerene to study the spectroscopic, electronic, and thermodynamic behaviors of the final complexes to verify whether or not the $B_{12}N_{12}$ fullerene is a suitable vector for the delivery of IFO drug.

## 2. Computational method

The calculations of total energies and optimization of geometric structures including $B_{12}N_{12}$, $B_{12}N_6C_6$, and $B_6N_6C_{12}$ fullerenes were carried out using the density functional theory (DFT) as implemented in the Gaussian 09 program package [36]. Also, a computational test was performed to investigate the effects of different methods and basis sets on the optimized geometrical structures. Two exchange-correlation functions were used within the DFT framework. First, the generalized gradient approximation (GGA) with the Perdew–Burke–Ernzerhof (PBE) [37], and then, the hybrid one parameter functional using modified hybrid M06-2X functional [38] were implemented indicating a higher percentage of HF (Hartree-Fock) exchange (54%). The M06-2X and PBE1 functions were chosen due to their good performance in calculations of the $C_{24}$, $B_{12}N_{12}$, Graphene, and MgO nanostructures [39–42], and the optimized geometric parameters (bond lengths and bond angles) are in excellent agreement with experimental results [43,44]. All binding energies ($E_b$) could be evaluated by zero-point corrected energies (ZPE), using the following equations:

$$E_b = (E_{IFO-Fullerene} + ZPE) - E_{Fullerene} - (EIFO + ZPE) \qquad (1)$$

$$E_b = (E_{IFO-Doped-Fullerene} + ZPE) - E_{Doped-Fullerene} - (E_{IFO} + ZPE) \qquad (2)$$

where $E_{IFO-Fullerene}$ and $E_{IFO-Doped-Fullerene}$ are the total energies of IFO drug over the $B_{12}N_{12}$, $B_{12}N_6C_6$, and $B_6N_6C_{12}$ fullerenes. $E_{IFO}$ is the total energy of the IFO drug and $E_{Fullerene}$ and $E_{Doped-Fullerene}$ are the total energies of the $B_{12}N_{12}$, $B_{12}N_6C_6$, and $B_6N_6C_{12}$ fullerenes. At least 30 lowest energy electronic excited states were computed for all the molecules. The energy convergence criteria were set about $10^{-6}$ eV where the optimized structures were achieved by force minimization about $10^{-4}$ eV/ Å. The time-dependent density functional theory (TDDFT) calculations were performed to achieve the crucial excited states of the related structures, and the differences of their dipole moments between the ground state and crucial excited state were evaluated using the same functional (M06-2X) and basis set (6-311 + G**) [45,46]. The PBE1/6-311 + G** level of theory is used for the calculation of the natural bond orbital (NBO) charges of the systems. Vibrational frequencies were calculated by the PBE and M06-2X functionals and used to first verify the nature of stationary points and second, to use the sum of electronic and thermal enthalpy. This includes electronic energy and translational, rotational, and thermal vibrational corrections for calculating the heat of the molecule formation, the sake of their future experimental identification by infrared (IR) spectroscopy, and the assignment of the observed frequencies. The quantum molecular descriptors (QMDs) were computed accordingly at the PBE and M06-2X functionals as follows:

$$\mu = -(I + A)/2 \qquad (3)$$

$$X = -\mu \qquad (4)$$

$$\eta = (I - A)/2 \qquad (5)$$

$$\omega = (\mu^2/2\eta) \qquad (6)$$

$$S = 1/2\eta \qquad (7)$$

Electronegativity ($X$) is determined as the negative of chemical potential ($\mu$), as follows: $= X\mu$. In addition, the chemical hardness ($\eta$)

can be determined using the Koopmans' theorem. I ($-E_{HOMO}$) is the ionization potential and A ($-E_{LUMO}$) the electron affinity of the molecule.

## 3. Results and discussion

### 3.1. The structures of $B_{12}N_{12}$, $B_{12}C_6N_6$, and $B_6C_{12}N_6$

The geometric structures and the frontier molecular orbital (FMO) of perfect $B_{12}N_{12}$, $B_{12}N_6C_6$, and $B_6N_6C_{12}$ are given in Fig. 1. The $T_h$ symmetrical $B_{12}N_{12}$ fullerene with a high thermodynamics stability ($\Delta G < 0$, $-1.87$ eV) [47] have two B–N bonds that consist of eight 6-membered rings (6-MR) and six 4-membered rings (4-MR) (Fig. 1). Because of the large iconicity of the boron-nitrogen bond in the perfect $B_{12}N_{12}$ fullerene, boron atoms with a charge of 0.185 |e| act as cations, while nitrogen atoms with a charge of $-0.185$ |e| act as anions at the PBE functional [48]. Within squares of $B_{12}N_{12}$, the bond distances are a bit larger than out of the squares (hexagons), 1.483, 1.486, and 1.493 Å versus 1.437, 1.438, and 1.446 Å, calculated at the M06-2X, PBE, and B3PW91 functionals, respectively. The results agree with previous theoretical calculations [49,50]. Table 1 shows non-equivalent atoms of $B_{12}N_6C_6$ fullerene in that the length of B–N, B–C, C–C, and C–N bonds within square rings are found to be 1.529, 1.521, 1.429, and 1.466 Å while in out of the squares are 1.415, 1.489, 1.407, and 1.410 Å by the PBE functional, respectively [51,52]. Energy gap ($E_g$) of $B_{12}N_{12}$, $B_{12}N_6C_6$, and $B_6N_6C_{12}$ fullerenes were estimated from the energy difference between the highest occupied molecular orbital (HOMO: $E_H$) and the lowest unoccupied molecular orbital (LUMO: $E_L$). It is worth noting that these orbitals are best termed as Kohn-Sham (KS) orbitals in DFT methods, which can be used to calculate ionization potentials (I = $-E_{HOMO}$) and electron affinities (A = $-E_{LUMO}$). The theoretical value of $E_g$ for $B_{12}N_{12}$ fullerene was calculated as 4.99, 6.71, and 9.45 eV by the PBE, B3LYP, and M06-2X functionals, and 6-311 + G** basis set, respectively, compared to similar results in previous studies [53–56]. Oku et al. experimentally calculated the $E_g$ (5.1 eV) of $B_{12}N_{12}$ fullerene [57]. In another study, Oku et al. showed an energy gap of about ~6.0 eV for boron nitride nanostructured materials [58] which indicates that PBE functional seems to correctly predict an $E_g$ for $B_{12}N_{12}$ fullerene in comparison with those of B3LYP and M06-2X functionals. Calculated TDOS plots demonstrate that $B_6N_6C_{12}$ and $B_{12}N_6C_6$ fullerenes are semiconductors with the $E_g$ values of 3.68 and 2.18 eV by the PBE/6-311 + G** level of theory, respectively. Li et al. [59] studied the electronic structure of $B_{12}N_{12}$ and $B_{12}N_6C_6$ fullerenes and calculated the values of $E_g$ for both fullerenes with amounts of 6.84 and 3.22 eV by the B3LYP/6-31G*, respectively. As shown in Fig. 1, the HOMO of $B_{12}N_{12}$ shows that the charge density is located on 2p orbital of nitrogen atom, while in the LUMO, the charge density is located on the 2p orbital of boron atom. In contrast with $B_{12}N_{12}$, the HOMO and LUMO of the $B_{12}N_6C_6$ and $B_6N_6C_{12}$ fullerenes indicate that the orbitals of boron and carbon show a better overlap than that of the orbitals of boron and nitrogen, showing a strong covalent character between them similar to previously reported calculations [59]. The values of quantum molecular descriptors (QMD) for the $B_{12}N_{12}$ adsorbent undergo changes when either of B or N atoms is substituted by a C atom (Table 2). The I and A values of the adsorbents decreased and increased, respectively. The decrease in the I value of the $B_{12}N_6C_6$ by the PBE and M06-2X functionals should be less than that of the $B_6N_6C_{12}$, and also the increase in the values of A for the $B_{12}N_6C_6$ should be greater than that of the $B_6N_6C_{12}$. The softness (S) and hardness ($\eta$) values also experienced increases and decreases making the $B_{12}N_6C_6$ and $B_6N_6C_{12}$ fullerenes more reactive species [60]. The values of hardness and softness are 2.50 and 0.20 eV for the $B_{12}N_{12}$ fullerene at the PBE functional, while these values at the M06-2X functional are 4.72 and 0.11 eV, respectively. Again, the S (0.46 eV) and $\eta$ (1.09 eV) values for the $B_{12}N_6C_6$ underwent more changes compared to that of the $B_6N_6C_{12}$ fullerene (S: 0.27 eV and $\eta$: 1.84 eV), which clearly reveals the effect of carbon substitution on these properties. Moreover, the values of $\omega$ and $D_M$ show that the $B_{12}N_6C_6$ is more capable of accepting random electrons from the moiety and has higher polarity than the $B_6N_6C_{12}$ hybrid adsorbent [61].

### 3.2. IFO adsorption on $B_{12}N_{12}$ and $B_6N_6C_{12}$ fullerenes

Fig. 2 illustrates various orientations of IFO adsorption upon a $B_{12}N_{12}$ fullerene by changing their separation distance before concluding about the best optimized geometry using M06-2X, B3PW91, and PBE1 methods. In this study, $B_{12}N_{12}$ is chosen as a base material for the IFO drug delivery. Furthermore, the motivation of the present work is to calculate the adsorption energy, energy gap variation, charge transfer, and electron density variation of the $B_{12}N_{12}$ fullerene on drug adsorption and desorption. When IFO drug from its phosphoryl head reacts with the boron atom of $B_{12}N_{12}$ fullerene (see state X), it results in a strong bond formed between IFO and the $B_{12}N_{12}$ with an $E_b$ value of $-1.21$ eV and a bond distance of 1.512 Å using M06-2X method. The interaction process to form complex **X** is an exothermic reaction with the changes in Gibbs free energy ($\Delta G$) and enthalpy ($\Delta H$) values of about $-2.50$ and $-3.07$ eV, respectively. Through the $\Delta G$ and $\Delta H$ values are larger than that of the complexes **K** and **Z** by the PBE functional in comparison with the M06-2X functional. The strong chemical interaction of the boron-phosphoryl bond in the IFO/$B_{12}N_{12}$ complex is due to strong anionic character of oxygen atom as shown by its negative charge from Mulliken population analysis ($-0.199$ |e|) [62]. We calculated the zero-point energy (ZPE) for the IFO drug from its phosphoryl head reaction with the $B_{12}N_{12}$ fullerene using M06-2X method. The values of ZPE in the most stable configuration of an isolated IFO drug adsorbed upon $B_{12}N_{12}$ fullerene are about $-0.12$ (state **K**), $-0.94$ eV (state **X**), and $-0.84$ (state **Z**), while these values in the PBE functional are $-0.16$ (state **K**), $-1.02$ eV (state **X**), and $-0.95$ (state **Z**). The small nearest atom distances (~1.512 Å) between the drug and the $B_{12}N_{12}$ present the possibility of covalent bond formation unlike $C_{60}$ fullerene with IFO that reveals weak
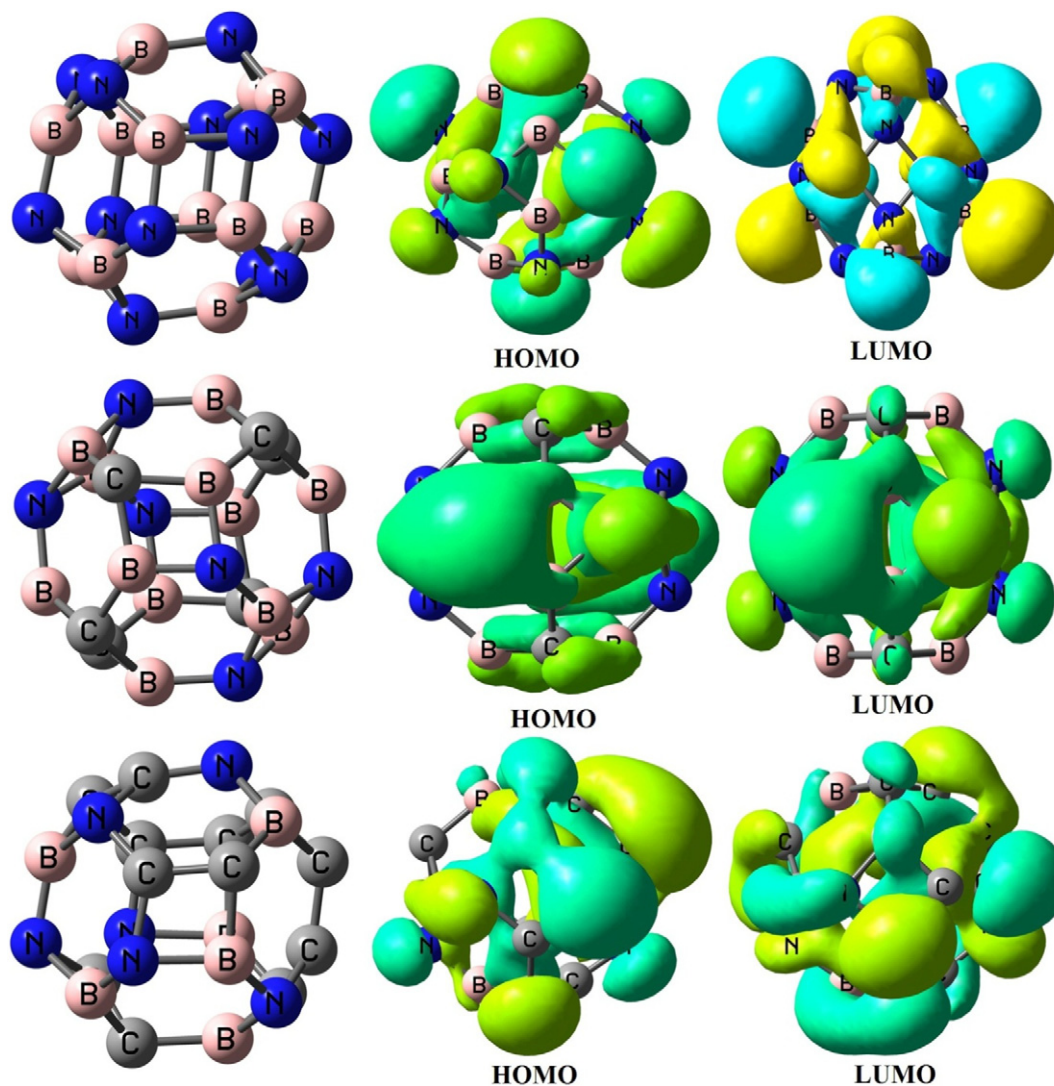
**Fig. 1.** Isosurfaces of the HOMO and LUMO orbitals of $B_{12}N_{12}$, $B_{12}N_6C_6$, and $B_6N_6C_{12}$ fullerenes.

and non-covalent interactions [63]. Khalifi et al. theoretically reported the interaction of IFO drug on the outer surface of the boron nitride nanotube (BNNT) by the PBE functional [64]. They reported an adsorption energy of −0.17 eV for this complex. However, the energy provided for IFO drug through phosphoryl upon $B_{12}N_{12}$ could be more stabilized than

$C_{60}$ fullerene and BNNT. Vibration spectra demonstrated that the P=O (1106 cm$^{-1}$) mode shifted to a lower frequency, and C–N (1190 cm$^{-1}$) and C–Cl (780 cm$^{-1}$) modes sifted to higher frequencies when IFO drug loaded on the surface of $B_{12}N_{12}$ fullerene compared with the pure IFO drug [65]. Theoretical stretching vibration of the P=O bond in IFO

**Table 1**
The structure parameters of the fullerenes in the different methods.

| Property | B–N/Å | B–C/Å | N–C/Å | C–C/Å | N–B–N/° | C–B–N/° | B–C–C/° | Diameter/Å |
|---|---|---|---|---|---|---|---|---|
| **Gas** | | | | | | | | |
| **PBE1** | | | | | | | | |
| $B_{12}N_{12}$ | 1.493 | – | – | – | 98.5 | – | – | 3.95 |
| $B_{12}N_6C_6$ | 1.478 | 1.543 | – | – | 124.7 | 99.1 | – | 4.09 |
| $B_6N_6C_{12}$ | 1.522 | 1.516 | 1.451 | 1.423 | 125.5 | 93.0 | 83.2 | 4.07 |
| **M06-2X** | | | | | | | | |
| $B_{12}N_{12}$ | 1.483 | – | – | – | 98.6 | – | – | 3.92 |
| $B_{12}N_6C_6$ | 1.498 | 1.529 | 1.461 | 1.397 | 124.1 | 95.2 | – | 4.04 |
| $B_6N_6C_{12}$ | 1.537 | 1.546 | 1.429 | 1.385 | 125.3 | 92.8 | 79.2 | 4.05 |
| **Water** | | | | | | | | |
| **PBE1** | | | | | | | | |
| $B_{12}N_{12}$ | 1.494 | – | – | – | 98.5 | – | – | 3.95 |
| $B_{12}N_6C_6$ | 1.481 | 1.501 | – | – | 126.2 | 107.4 | – | 3.89 |
| $B_6N_6C_{12}$ | 1.497 | 1.531 | 1.457 | 1.400 | 124.1 | 95.0 | 79.2 | 4.05 |
| **M06-2X** | | | | | | | | |
| $B_{12}N_{12}$ | 1.483 | – | – | – | 125.8 | – | – | 3.92 |
| $B_{12}N_6C_6$ | 1.479 | 1.496 | – | – | 125.9 | 107.5 | – | 3.88 |
| $B_6N_6C_{12}$ | 1.497 | 1.533 | 1.462 | 1.394 | 124.2 | 95.2 | 79.0 | 4.05 |

**Table 2**
Electronic properties of the fullerenes in the different methods.

| Property | $E_H$/eV | $E_L$/eV | $E_g$/eV | $E_F$/eV | $\Delta E_g$/eV | I/eV | A/eV | $\eta$/eV | S/eV | $\mu$/eV | $\omega$/eV | $D_M$/Debye |
|---|---|---|---|---|---|---|---|---|---|---|---|---|
| **Gas** | | | | | | | | | | | | |
| **PBE1** | | | | | | | | | | | | |
| $B_{12}N_{12}$ | −7.03 | −2.04 | 4.99 | −4.54 | – | 7.03 | 2.04 | 2.50 | 0.20 | −4.54 | 4.12 | 0.0 |
| $B_{12}N_6C_6$ | −6.97 | −4.79 | 2.18 | −5.88 | 56.31 | 6.97 | 4.79 | 1.09 | 0.46 | −5.88 | 15.86 | 2.54 |
| $B_6N_6C_{12}$ | −6.76 | −3.08 | 3.68 | −4.92 | 26.25 | 6.76 | 3.08 | 1.84 | 0.27 | −4.92 | 6.58 | 2.37 |
| **M06-2X** | | | | | | | | | | | | |
| $B_{12}N_{12}$ | −9.46 | −0.01 | 9.45 | −4.74 | – | 9.46 | 0.01 | 4.72 | 0.11 | −4.74 | 2.37 | 0.0 |
| $B_{12}N_6C_6$ | −7.98 | −3.70 | 4.28 | −5.84 | 54.71 | 7.98 | 3.70 | 2.14 | 0.23 | −5.84 | 7.97 | 3.17 |
| $B_6N_6C_{12}$ | −7.75 | −2.30 | 5.45 | −5.03 | 42.33 | 7.75 | 2.30 | 2.73 | 0.18 | −5.03 | 4.63 | 2.47 |
| **Water** | | | | | | | | | | | | |
| **PBE1** | | | | | | | | | | | | |
| $B_{12}N_{12}$ | −8.27 | −0.87 | 7.40 | −4.57 | – | 8.27 | 0.87 | 3.70 | 0.14 | −4.57 | 2.82 | 0.0 |
| $B_{12}N_6C_6$ | −6.81 | −5.05 | 1.76 | −5.93 | 76.22 | 6.81 | 5.05 | 0.88 | 0.57 | −5.93 | 19.98 | 0.0 |
| $B_6N_6C_{12}$ | −6.72 | −2.96 | 3.76 | −4.84 | 49.19 | 6.72 | 2.96 | 1.88 | 0.27 | −4.84 | 6.23 | 4.42 |
| **M06-2X** | | | | | | | | | | | | |
| $B_{12}N_{12}$ | −9.51 | −0.29 | 9.22 | −4.90 | – | 9.51 | 0.29 | 4.61 | 0.11 | −4.90 | 2.60 | 0.0 |
| $B_{12}N_6C_6$ | −7.93 | −4.39 | 2.94 | −5.86 | 68.11 | 7.93 | 4.39 | 1.77 | 0.28 | −6.16 | 10.72 | 0.01 |
| $B_6N_6C_{12}$ | −7.70 | −2.18 | 5.52 | −4.94 | 40.13 | 7.70 | 2.18 | 2.76 | 0.18 | −4.94 | 4.42 | 4.28 |

drug is observed in the region 1137–1292 cm$^{-1}$ by the PBE functional, which is lower than the experimental data (1140-1300 cm$^{-1}$) [66]. This result can contribute to the interaction of the drug from its P=O group when close to boron atom of the adsorbent. Nevertheless, the state **K** exhibits a weak chemical interaction (or non-covalent interactions) between IFO from its chloroalkyl head ($E_b$ = −0.35 eV) and the boron atom of $B_{12}N_{12}$ fullerene with an interaction distance of 2.828 Å. When IFO from its nitrogen head was close to the surface of boron atom of $B_{12}N_{12}$ fullerene (**see state Z**), it had a $E_b$ value with interaction distances of −1.14 eV and 1.684 Å, respectively, representing that the IFO drug from its phosphoryl head is more stable than those of the chloroalkyl and nitrogen heads. Fig. 3 presents the most stable interaction configurations between the IFO drug from its phosphoryl head and $B_6N_6C_{12}$ fullerene in the most stable configuration. As shown in Table 2, a strong chemical bond was formed between the IFO drug and the $B_6N_6C_{12}$ fullerene with an $E_b$ value of −2.06 eV and an interaction distance of 1.504 Å by the M06-2X functional. At the PBE1 functional, however, the $E_b$ value between the drug and the $B_6N_6C_{12}$ fullerene increased to −2.60 eV with an interaction distance of 1.468 Å, suggesting a strong chemical interaction (or chemisorption) between the drug and the fullerene, similar to that of Loh et al. [67]. The values of $E_b$ and the interaction distances between the IFO drug and $B_{12}N_6C_6$ fullerene are about −1.61 eV and 1.491 Å by the PBE functional and −1.48 eV and 1.520 Å by the M06-2X functional, respectively.

The value of dipole moment ($D_M$) for $B_{12}N_6C_6$ further increased upon the adsorption of IFO drug in water environment (M06-2X: 23.67 Debye and PBE: 22.27 Debye) than the vacuum environment (M06-2X: 15.56 Debye and PBE: 22.68 Debye). The values of ΔG for the $B_{12}N_6C_6$ and $B_6N_6C_{12}$ fullerenes with the IFO drug were obtained as −0.98 and −0.66 eV, while the values of ΔH for these complexes were −1.50 and −1.28 eV, respectively. The lesser value of ΔG than that of ΔH is because of the entropic effect suggesting that interactions of IFO drug on both $B_{12}N_6C_6$ and $B_6N_6C_{12}$ fullerenes are thermodynamically possible. Our observations indicated that the pure $B_{12}N_6C_6$ and $B_6N_6C_{12}$ fullerenes had strong interactions with IFO drug with large $E_b$ values and small interaction distances. This fact is supported by the calculated large amounts of charge transfer between the drug and the pure fullerenes. The value of ZPE in the most stable configurations of an isolated IFO drug adsorbed upon $B_6N_6C_{12}$ and $B_{12}N_6C_6$ fullerenes are about −1.92 and −1.19 eV in the states **L** and **J** by the M06-2X functional, while these values are −2.01 and −1.32 eV at the PBE functional, respectively. Vibration spectra showed that the P=O and B–N modes shifted to lower frequencies in $B_6N_6C_{12}$ (1101 and 1318 cm$^{-1}$) and $B_{12}N_6C_6$ (1099 and 1316 cm$^{-1}$) when IFO drug loaded on the surface of fullerenes.

The values of QMD for the adsorbents (See Tables 3 and 4) underwent some changes due to their interactions with IFO. There were decreased ionization potential (I) values but increased electron affinity (A) values because of the electrons shared from IFO to the adsorbents. This phenomenon increased the number of outer electrons on the adsorbent and lowered the affinity of these electrons to the nucleus of the B and N atoms. There were also decreased and increased hardness (η) and softness (S) values, which denote more reactivity of the final IFO-adsorbent complexes after the interaction process. The increased chemical potential (μ) and electrophilicity index (ω) show more reactivity of the complexes and also capability of the resultant complexes to accept random number of electrons, which reduces the toxicity of the complexes and increases their biocompatibility [68].

### 3.3. Solvation energies

The polarizable continuum model (PCM) was studied for the solvent effect [69], where the water (H$_2$O) with a dielectric constant of 78.30 as the most abundant biological
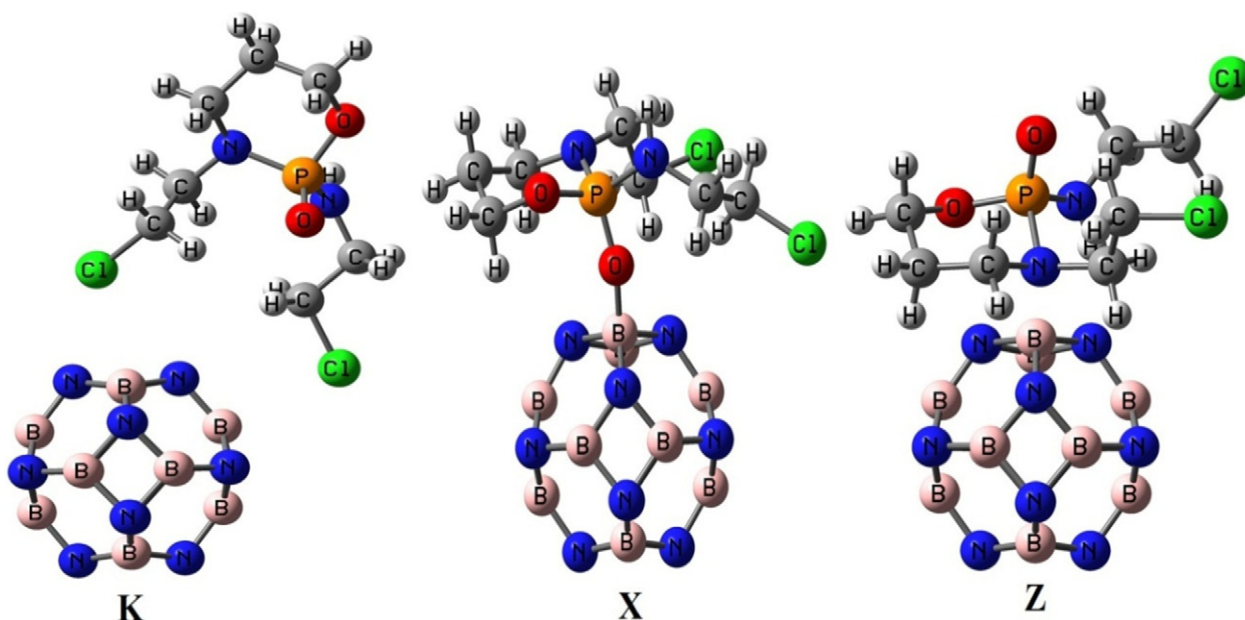


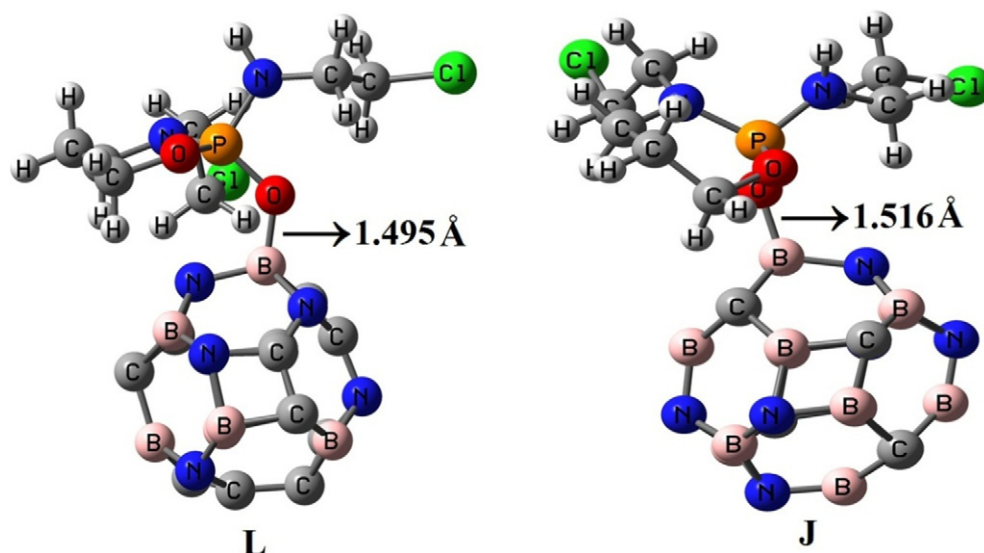**Fig. 2.** IFO adsorbed on the surface of $B_{12}N_{12}$ fullerene.

**Fig. 3.** IFO adsorbed on the surfaces of $B_{12}N_6C_6$ and $B_6N_6C_{12}$ fullerenes.

**Table 3**
The structure and electronic parameters of the fullerenes interacting with IFO by the M06-2X functional.

| Property | Diameter/Å | $E_H$/eV | $E_L$/eV | $E_g$/eV | $E_F$/eV | I/eV | A/eV | η/eV | S/eV | μ/eV | ω/eV | $D_M$/Debye |
|---|---|---|---|---|---|---|---|---|---|---|---|---|
| K | 3.92 | −8.69 | −0.31 | 8.38 | −4.50 | 8.69 | 0.31 | 4.19 | 0.12 | −4.50 | 2.42 | 7.68 |
| X | 4.20 | −8.36 | −0.74 | 7.62 | −4.55 | 8.36 | 0.74 | 3.81 | 0.13 | −4.55 | 2.72 | 12.63 |
| Z | 4.19 | −8.95 | −0.46 | 8.49 | −4.71 | 8.95 | 0.46 | 4.25 | 0.12 | −4.71 | 2.61 | 4.35 |

**Table 4**
The structure and electronic parameters of the doped fullerenes interacting with IFO by the PBE1 and M06-2X functionals.

| Property | Diameter/Å | $E_H$/eV | $E_L$/eV | $E_g$/eV | $E_F$/eV | I/eV | A/eV | η/eV | S/eV | μ/eV | ω/eV | $D_M$/Debye |
|---|---|---|---|---|---|---|---|---|---|---|---|---|
| **PBE** | | | | | | | | | | | | |
| L | 4.35 | −6.19 | −2.26 | 3.93 | −4.23 | 6.19 | 2.26 | 1.97 | 0.25 | −4.23 | 4.54 | 22.68 |
| J | 4.33 | −5.82 | −3.85 | 1.97 | −4.84 | 5.82 | 3.85 | 0.99 | 0.51 | −4.84 | 11.87 | 10.68 |
| **M06-2X** | | | | | | | | | | | | |
| L | 4.34 | −6.73 | −1.27 | 5.46 | −4.00 | 6.73 | 1.27 | 2.73 | 0.18 | −4.00 | 2.93 | 15.56 |
| J | 4.47 | −7.04 | −2.38 | 4.66 | −4.71 | 7.04 | 2.38 | 2.33 | 0.21 | −4.71 | 4.76 | 8.38 |

molecule was selected as the solvent [70]. The differences between the optimized energies in the water and vacuum environments for the most stable adsorption configurations were calculated and defined as the $E_{solv}$. A more negative $E_{solv}$ demonstrate that solvation is a spontaneous process and also signify the stability of the investigated systems in the water environment. The calculated $E_{solv}$ value in the interaction between IFOS and

$B_{12}N_{12}$ demonstrates a strong chemical interaction with an energy of about −1.27 eV by the PBE1 functional and −1.41 eV by the M06-2X functional. The covalent interaction study of $B_{12}N_{12}$ fullerene was further examined by taking two IFOS drugs in both functionals (See Fig. 4). When two IFOS drugs chemisorbed on the fullerene surface, $E_{solv}$ value slightly reduced after the interaction between two species, which shows good
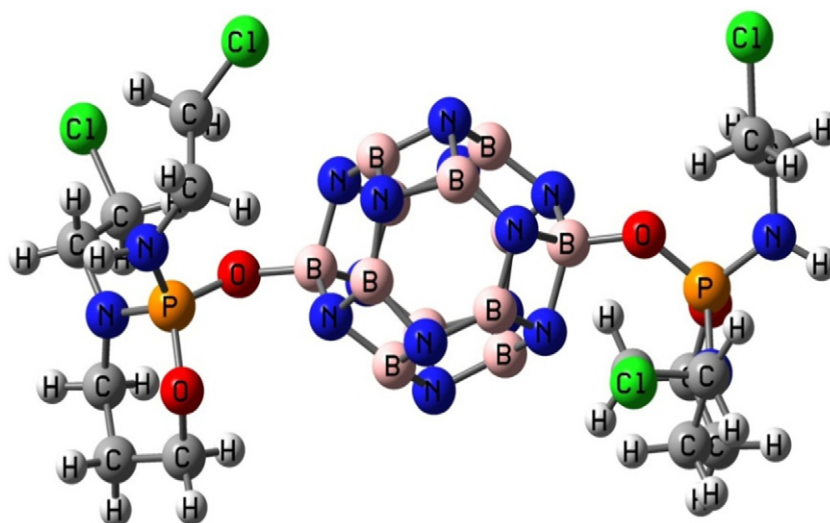


**Fig. 4.** IFO adsorbed on the surfaces of $B_{12}N_{12}$ fullerene.

agreement with other works [18,39]. When two IFOS drugs chemisorbed on the outer surface of fullerene, a distance of 1.518 Å and a release of −1.14 eV energy for per drug observed by the PBE1 functional. However, a chemisorption of −1.25 eV was found for per drug at the M06-2X functional.

In the next step, the covalent binding of the $B_{12}N_6C_6$ and $B_6N_6C_{12}$ fullerenes with IFOS drug is evaluated and reported for both functionals. First, increased polarity of carbon-doped $B_{12}N_{12}$ fullerene raises its solubility in a polar solvent. As it is clear from Table 4, optimization of the selected configurations in water results in the stabilization of the adsorption configurations due to the interaction of hydrophilic IFO with water, which is thermodynamically more favorable than the same interaction configuration in the vacuum phase resulting in increases and decreases of the binding energies between IFO and fullerenes and the bond lengths of fullerene-drug complexes, respectively. In case of IFO adsorption in water environment for the $B_{12}N_6C_6$ and $B_6N_6C_{12}$ fullerenes, the $E_{solv}$ rises to −1.86 and −1.99 eV with the distances of 1.491 and 1.468 Å, respectively. The calculated dipole moment value rises from 0.0 to 4.42 Debye in the $B_{12}N_6C_6$ and $B_6N_6C_{12}$ fullerenes to 14.58 and 22.67 Debye in the IFO/$B_{12}N_6C_6$ and IFO/$B_6N_6C_{12}$ complexes in water environment. Structures with higher polarities show more stability in water, hence the more negative $E_{solv}$ results in a higher degree of solubility. The values of the QCM

parameters are somewhat bigger almost in all cases calculated in water phase compared to those of QCM parameters in the vacuum phase. Moreover, the values obtained for the QCM parameter at the PBE (water) functional are smaller than those of M062X (water). These results indicate that the presence of water is a more preferred phase to facilitate the IFO interaction with the applied hybrid fullerenes.

### 3.4. Electronic properties

Fig. 5(a) depicts the color-filled maps of electron density (ED) and the projected density of states (PDOS) of the considered systems. For IFOS adsorbed on the $B_{12}N_{12}$ fullerene, a system is observed with large energy gap in which each fragment (frags1 and 2 indicate the $B_{12}N_{12}$ fullerene and IFO molecule, respectively) has the electronic density of state localized around the HOMO and LUMO states. According to the figure, the LUMO ($E_L$) and HOMO ($E_H$) states of the $B_{12}N_{12}$/IFO were strongly affected by the $B_{12}N_{12}$ electronic structure. The energy gap of $B_{12}N_{12}$ fullerene shifts from 4.99 eV to 2.18 and 3.68 eV for the $B_{12}N_6C_6$ and $B_6N_6C_{12}$ fullerenes, respectively, by the PBE functional, while the $E_g$ of $B_{12}N_{12}$ fullerene at the M06-2X functional shifts from 9.45 eV to 4.28 and 5.45 eV for both fullerenes in vacuum environment, respectively. However, these changes in water
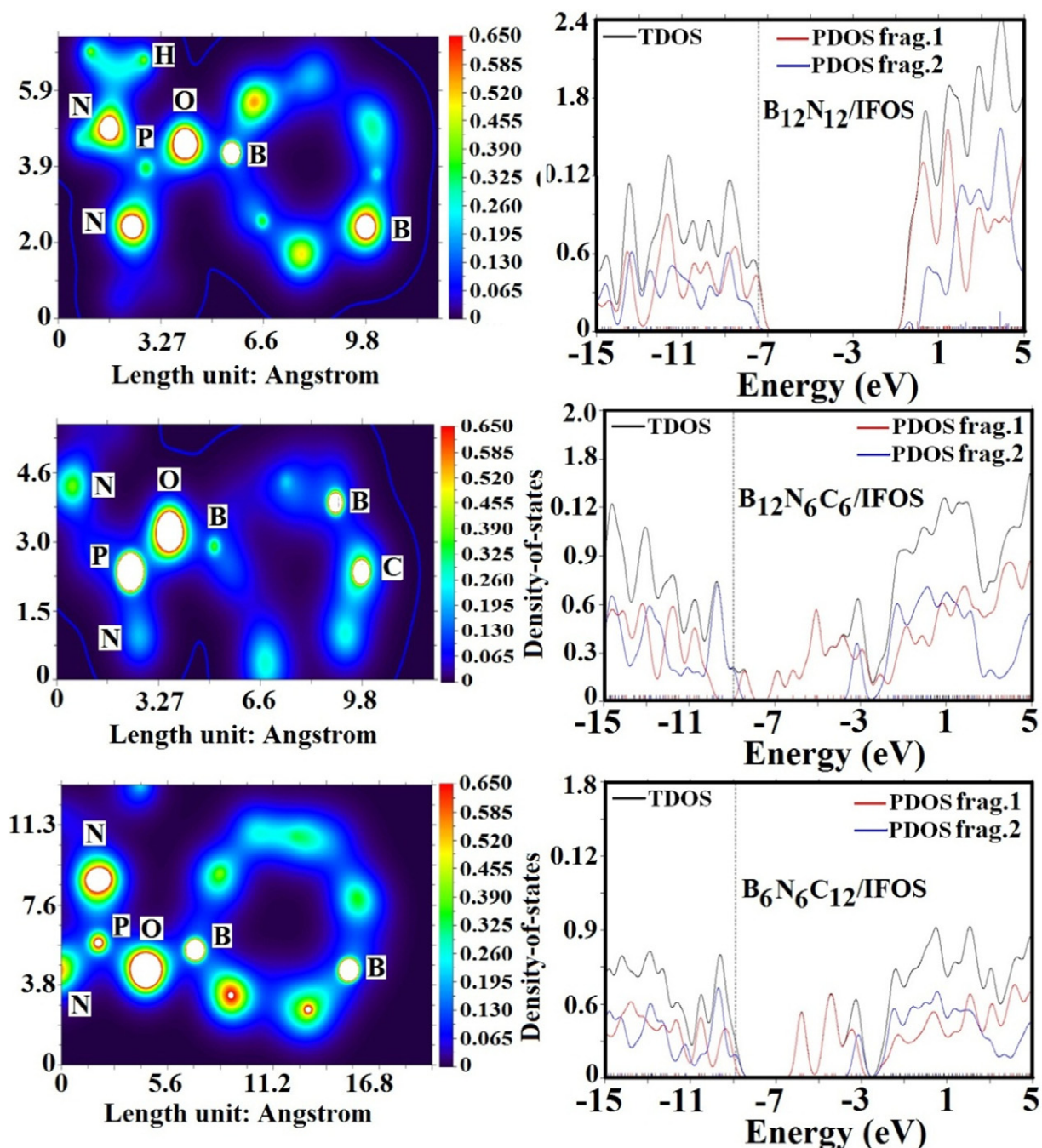


**Fig. 5.** ED and PDOS plots of IFO adsorbed on the surfaces of pure, $B_{12}N_6C_6$ and $B_6N_6C_{12}$ fullerenes.

**Table 5**

The structure and electronic parameters of the doped fullerenes interacting with IFO by the PBE1 and M06-2X functionals in water environment.

| Property | Diameter/Å | $E_H$/eV | $E_L$/eV | $E_g$/eV | $E_F$/eV | I/eV | A/eV | $\eta$/eV | S/eV | $\mu$/eV | $\omega$/eV | $D_M$/Debye |
|---|---|---|---|---|---|---|---|---|---|---|---|---|
| **PBE** | | | | | | | | | | | | |
| L | 4.38 | −6.20 | −2.66 | 3.54 | −4.43 | 6.20 | 2.66 | 1.77 | 0.28 | −4.43 | 5.54 | 22.27 |
| J | 4.37 | −6.15 | −4.18 | 1.97 | −5.17 | 6.15 | 4.18 | 0.99 | 0.51 | −5.17 | 13.54 | 14.58 |
| **M06-2X** | | | | | | | | | | | | |
| L | 4.35 | −7.18 | −1.55 | 5.63 | −4.36 | 7.18 | 1.55 | 2.82 | 0.18 | −4.37 | 3.38 | 23.67 |
| J | 4.44 | −7.11 | −2.15 | 4.96 | −4.63 | 7.11 | 2.15 | 2.48 | 0.20 | −4.63 | 4.32 | 16.58 |

environment was found to be larger than those in vacuum environment (See Table 2). As shown in Tables 3–5, the electronic structures of $B_{12}N_6C_6$ fullerene is considerably affected by the adsorption of IFO drug in both environments compared to $B_{12}N_{12}$ and $B_6C_6N_{12}$ fullerenes. Thus, $B_{12}N_6C_6$ fullerene can produce an electrical noise in the presence of IFO drug and may be applied as biosensor for medical application and their performance for the detection of anticancer drugs. Regarding the ED plot of the $B_{12}N_{12}$/IFO system, the active point on the drug molecule at HOMO state is related to the B and N atoms near to the surface of the $B_{12}N_{12}$ fullerene. For the $B_{12}N_6C_6$/IFO system, there is a significant deformation of the molecular structure that affected the corresponding electronic structure of the system. As shown in Fig. 5(b), the mid gap states appear in a wide range of energies in the form of unlocalized state for the $B_{12}N_{12}$ fragment and localized donoric state of the IFO molecule. The ED plot of the $B_{12}N_6C_6$/IFOS indicates the active points on the molecule as C, B, and N atoms. The same situation can also be seen for the $B_6C_6N_{12}$/IFO system in Fig. 5(c), where the mid gap states are made according to the broken degenerated states while the new states have a localized form. The localized form of the edge states can be clearly understood from ED plot of the $B_6C_6N_{12}$/IFO system where the ED significantly is localized on the nitrogen atoms.

## 4. Concluding remarks

In summary, based on the density functional theory and the time-dependent density functional theory calculations, the adsorption of IFO through different functional groups upon the $B_{12}N_{12}$ fullerene was evaluated by the M06-2X and PBE1 functionals for both gas and water environments. The adsorption of IFO through phosphoryl group (−1.21 eV) increased significantly onto the $B_{12}N_{12}$ in comparison with chloroalkyl (−0.35 eV) and nitrogen atom of oxazaphosphorine ring (−1.14 eV) groups. Our theoretical results demonstrate that covalent functionalization of fullerene surfaces with IFO (through P=O group) are thermodynamically favorable due to the remarkable adsorption energies, so we conclude that the fullerene–IFO complexes are quite stable. It was found that the IFO from its phosphoryl group could only be adsorbed chemically on the boron atom of $B_{12}N_6C_6$ (−1.86 eV) and that $B_6N_6C_{12}$ (−1.99 eV) fullerenes were larger than those on the pure $B_{12}N_{12}$ fullerene. Between both environments, in contrast, adsorption of IFO through P=O group onto $B_{12}N_6C_6$ and $B_6N_6C_{12}$ fullerenes in water environment demonstrated higher energy, which was lower than that of the vacuum environment, while the energy rose in the pure fullerene. The changes of electronic structure of $B_{12}N_{12}$, $B_{12}N_6C_6$, and $B_6N_6C_{12}$ fullerenes represented that IFO adsorption onto fullerenes raised their chemical reactivity. The values of dipole moment for $B_{12}N_{12}$, $B_{12}N_6C_6$, and $B_6N_6C_{12}$ fullerenes increased upon the adsorption of IFO in water environment compared with the vacuum environment. Based on our calculations, the improved binding energy and dipole moment reduced $E_g$ for IFO interacting with $B_{12}N_6C_6$ surface compared with the $B_{12}N_{12}$ and $B_6N_6C_{12}$ fullerenes for both gas and water environments. It was observed that the IFO adsorption on the $B_{12}N_6C_6$ led to a large distortion on the substrate surface and broadened their $E_g$ values remarkably in comparison to the $B_6N_6C_{12}$ fullerenes, which seems quite plausible for the detection of IFO. Consequently, chemical modification of fullerene surfaces using covalent functionalization scheme is an efficacious approach that is promising for loading and delivery of drug molecules, therapeutics, and biomolecules.

## Acknowledgment

## References

[1] T. Oku, A. Nishiwaki, I. Narita, Sci. Technol. Adv. Mater. 5 (2004) 629.
[2] S.M. Lee, Y.H. Lee, Y.G. Hwang, J. Elsner, D. Porezag, T. Frauenheim, Phys. Rev. B Condens. Matter 60 (1999) 7788.
[3] G. Seifert, E. Hernandez, Chem. Phys. Lett. 318 (2000) 355.
[4] H.S. Wu, F.Q. Zhang, X.H. Xu, C.J. Zhang, H. Jiao, J. Phys. Chem. A 107 (2003) 204.
[5] C. Balasubramanian, S. Belluci, P. Castrucci, M.D. Crescenzi, S.V. Bhoraskar, Chem. Phys. Lett. 383 (2004) 188.
[6] L. Bourgeois, Y. Bando, W.Q. Han, T. Sato, Phys. Rev. B Condens. Matter 61 (2000) 7686.
[7] J.J. Belbruno, Chem. Phys. Lett. 313 (1999) 795.
[8] T.R. Taylor, K.R. Asmis, C. Xu, D.M. Neumark, Chem. Phys. Lett. 297 (1998) 133.
[9] N.G. Chopra, et al., Science 269 (1995) 966.
[10] D. Golberg, Y. Bando, O. St_ephan, K. Kurashima, Appl. Phys. Lett. 73 (1998) 2441.
[11] D. Golberg, Y. Bando, K. Kurashima, T. Sato, Scr. Mater. 44 (2001) 1561.
[12] D.-B. Zhang, E. Akatyeva, T. Dumitrica, Phys. Rev. B Condens. Matter Mater. Phys. 84 (2011) 115431.
[13] J.M. Matxain, L.A. Eriksson, J.M. Mercero, X. Lopez, M. Piris, J.M. Ugalde, J. Poater, E. Matito, M. Sola, New solids based on B12N12 fullerenes, J. Phys. Chem. C 111 (2007) 13354–13360.
[14] A.V. Pokropivny, Structure of the boron nitride E-phase: diamond lattice of B12N12 fullerenes, Diam. Relat. Mater. 15 (2006) 1492–1495.
[15] A. Soltani, M. Bezi Javan, Carbon monoxide interactions with pure and doped $B_{11}XN_{12}$ (X=Mg, Ge, Ga) nano-cluster: a theoretical study, RSC Adv. 5 (2015) 90621–90631.
[16] V.V. Pokropivny, V.V. Skorokhod, G.S. Oleinik, A.V. Kurdyumov, T.S. Bartnitskaya, A.V. Pokropivny, A.G. Sisonyuk, D.M. Sheichenko, Boron nitride analogs of fullerenes (the fulborenes), Nanotubes,and fullerites (the fulborenites), J. Solid State Chem. 154 (2000) 214–222.
[17] A. Soltani, M.T. Baei, E. Tazikeh Lemeski, M. Shahini, Sensitivity of BN nano-cages to caffeine and nicotine molecules, Superlattice Microstruct. 76 (2014) 315–325.
[18] M. Bezi Javan, A. Soltani, E. Tazikeh Lemeski, A. Ahmadi, S. Moazen Rad, Interaction of $B_{12}N_{12}$ nano-cage with cysteine through various functionalities: a DFT study, Superlattice Microstruct. 100 (2016) 24–37.
[19] M.T. Baei, M. Ramezani Taghartapeh, E. Tazikeh Lemeski, A. Soltani, A computational study of adenine, uracil, and cytosine adsorption upon AlN and BN nano-cages, Physica B 444 (2014) 6–13.
[20] A. Soltani, A. Sousaraei, M. Bezi Javan, M. Eskandari, H. Balakheyli, Electronic and optical properties of 5-AVAfunctionalized BN nanoclusters: a DFT study, New J. Chem. 40 (2016) 7018–7026.
[21] M. Bezi Javan, A. Soltani, Z. Azmoodeh, N. Abdolahi, N. Gholami, A DFT study on the interaction between 5-fluorouracil and $B_{12}N_{12}$ nanocluster, RSC Adv. 6 (2016) 104513–104521.
[22] A. Soltani, M.T. Baei, M. Ramezani Taghartapeh, E. Tazikeh Lemeski, S. Shojaee, Phenol interaction with different nano-cages with and without an electric field: a DFT study, Struct. Chem. 26 (2015) 685–693.
[23] M. Solimannejad, S. Kamalinahad, M. Noormohammadbeigi, H. Jouypazadeh, Chemisorption of pyrimidine nucleotide onto exterior surface of pristine $B_{12}N_{12}$ nanocluster: a theoretical study, Phys. Chem. Res. 6 (2018) 1–14.
[24] A.S. Ghasemi, M. Ramezani Taghartapeh, A. Soltani, P.J. Mahon, Adsorption behavior of metformin drug on boron nitride fullerenes: thermodynamics and DFT studies, J. Mol. Liq. 275 (2019) 955–967.
[25] F. Rahimi, A. Zabaradsti, Photo-induced electron transfer process on pristine and Sc-substituted $B_{12}N_{12}$ nanocage as $H_2S$ chemosensor: a fully DFT and TD-DFT study, J. Inorg. Organomet. Polym. 27 (2017) 1770–1777.
[26] S. Yourdkhani, T. Korona, N.L. Hadipour, Structure and energetics of complexes of $B_{12}N_{12}$ with hydrogen halides-SAPT (DFT) and MP2 study, J. Phys. Chem. A 119 (2015) 6446–6467.
[27] E. Vessally, M.D. Esrafili, R. Nurazar, P. Nematollahi, A. Bekhradnia, A DFT study on electronic and optical properties of aspirin-functionalized $B_{12}N_{12}$ fullerene-like nanocluster, Struct. Chem. 28 (2017) 735–748.
[28] K. Hirabayashi, E. Okada, Cancer 71 (1993) 2769.
[29] A.F. Scinto, V. Ferraresi, M. Milella, E. Tucci, C. Santomaggio, R. Pasquali-Lasagni, M.R. Del-Vecchio, N. Campioni, M. Nardi, F. Cognetti, Br. J. Canc. 81 (1999) 1031.
[30] A. Perales, S. Garcia-Blanco, Acta Crystallogr. B33 (1977) 1935.
[31] S. Kilickap, M. Cakar, I.K. Onal, A. Tufan, H. Akoglu, S. Aksoy, M. Erman, G. Tekuzman, Ann. Pharmacother. 40 (2006) 332–335.

[32] R. Rossi, A. Gödde, A. Kleinebrand, M. Riepenhausen, J. Boos, J. Ritter, J. Clin. Oncol. 12 (1994) 159–165.

[33] R. Skinner, I.M.A. Sharkey, D.J. Pearson, A.W. Craft, J. Clin. Oncol. 11 (1993) 173–190.

[34] E. Duverger, T. Gharbi, E. Delabrousse, F. Picaud, Quantum study of boron nitride nanotubes functionalized with anticancer molecules, Phys. Chem. Chem. Phys. 16 (2014) 18425–18432.

[35] M. El Khalifi, E. Duverger, T. Gharbi, H. Boulahdour, F. Picaud, Theoretical use of boron nitride nanotubes as a perfect container for anticancer molecules, Anal. Methods 8 (2016) 1367–1372.

[36] D. 01, M.J. Frisch, G.W. Trucks, H.B. Schlegel, G.E. Scuseria, M.A. Robb, J.R. Cheeseman, G. Scalmani, V. Barone, B. Mennucci, G.A. Petersson, H. Nakatsuji, M. Caricato, X. Li, H.P. Hratchian, A.F. Izmaylov, J. Bloino, G. Zheng, J.L. Sonnenberg, M. Hada, M. Ehara, K. Toyota, R. Fukuda, J. Hasegawa, M. Ishida, T. Nakajima, Y. Honda, O. Kitao, H. Nakai, T. Vreven, J.A. Montgomery Jr., J.E. Peralta, F. Ogliaro, M. Bearpark, J.J. Heyd, E. Brothers, K.N. Kudin, V.N. Staroverov, R. Kobayashi, J. Normand, K. Raghavachari, A. Rendell, J.C. Burant, S.S. Iyengar, J. Tomasi, M. Cossi, N. Rega, J.M. Millam, M. Klene, J.E. Knox, J.B. Cross, V. Bakken, C. Adamo, J. Jaramillo, R. Gomperts, R.E. Stratmann, O. Yazyev, A.J. Austin, R. Cammi, C. Pomelli, J.W. Ochterski, R.L. Martin, K. Morokuma, V.G. Zakrzewski, G.A. Voth, P. Salvador, J.J. Dannenberg, S. Dapprich, A.D. Daniels, €O. Farkas, J.B. Foresman, J.V. Ortiz, J. Cioslowski, D.J. Fox, Gaussian 09, Revision, Gaussian, Inc., Wallingford CT, 2009.

[37] J.P. Perdew, K. Burke, M. Ernzerhof, Generalized gradient approximation made simple, Phys. Rev. Lett. 77 (1996) 3865.

[38] Y. Zhao, D.G. Truhlar, Theor. Chem. Acc. 120 (2006) 215–241.

[39] A. Soltani, M. Ramezani Taghartapeh, V. Erfani-Moghadam, M. Bezi Javan, F. Heidari, M. Aghaei, P.J. Mahon, Serine adsorption through different functionalities on the $B_{12}N_{12}$ and Pt-$B_{12}N_{12}$ nanocages, Mater. Sci. Eng. C 92 (2018) 216–227.

[40] A. Soltani, M. Bezi Javan, M.T. Baei, Z. Azmoodeh, Adsorption of chemical warfare agents over $C_{24}$ fullerene: effects of decoration of cobalt, J. Alloy. Comp. 735 (2018) 2148–2161.

[41] P. Lazar, F. Karlický, P. Jurečka, M. Kocman, E. Otyepková, K. Šafářová, M. Otyepka, Adsorption of small organic molecules on Graphene, J. Am. Chem. Soc. 135 (16) (2013) 6372–6377.

[42] A. Soltani, M. Ramezani Taghartapeh, M. Bezi Javan, P.J. Mahon, Z. Azmoodeh, E. Tazikeh Lemeski, I.V. Kityk, Theoretical studies of hydrazine detection by pure and Al defected MgO nanotubes, Phys. E 97 (2018) 239–249.

[43] M. Ramezani Taghartapeh, N. Noroozi Pesyan, H. Rashidnejad, H.R. Khavasi, A. Soltani, Synthesis, spectroscopic and photophysical studies of xanthene derivatives, J. Mol. Struct. 1149 (2017) 862–873.

[44] A. Soltani, M. Bezi Javan, S. Ghafouri Raz, R. Mashkoor, A. Dehno Khalaji, M. Dusek, K. Fejfarova, L. Palatinus, J. Rohlicek, P. Machek, Crystallography, vibrational, electronic and optical analysis of 4-Bromo-2-(2,5-dichloro-phenylimino)-phenol, J. Mol. Struct. 1173 (2018) 521–530.

[45] M. Niu, G. Yu, G. Yang, W. Chen, X. Zhao, X. Huang, Doping the alkali atom: an effective strategy to improve the electronic and nonlinear optical properties of the inorganic $Al_{12}N_{12}$ nanocage, Inorg. Chem. 53 (2014) 349–358.

[46] D. Jacquemin, E.A. Perpète, I. Ciofini, C. Adamo, Assessment of functionals for TD-DFT calculations of Singlet—Triplet transitions, J. Chem. Theory Comput. 6 (5) (2010) 1532–1537.

[47] H.-S. Wu, X.-H. Xu, F.-Q. Zhang, H. Jiao, New boron nitride $B_{24}N_{24}$ nanotube, J. Phys. Chem. A 107 (2003) 6609–6612.

[48] S.-H. Wen, W.-Q. Deng, K.-L. Han, Endohedral BN metallofullerene M@$B_{36}N_{36}$ complex as promising hydrogen storage materials, J. Phys. Chem. C 112 (2008) 12195–12200.

[49] E. Shakerzadeh, N. Barazesh, S. Zargar Talebi, A comparative theoretical study on the structural, electronic and nonlinear optical features of $B_{12}N_{12}$ and $Al_{12}N_{12}$ nanoclusters with the groups III, IV and V dopants, Superlattice Microstruct. 76 (2014) 264–276.

[50] F. Jensen, H. Toflund, Chem. Phys. Lett. 201 (1993) 89.

[51] Z. Zhou, J. Zhao, X. Gao, Z. Chen, J. Yan, P. von Rague Schleyer, M. Morinaga, Docomposite single-walled nanotubes have enhanced capability for lithium storage? Chem. Mater. 17 (2005) 992–1000.

[52] A. Soltani, Z. Azmoodeh, M. Bezi Javan, E. Tazikeh Lemeski, L. Karami, A DFT study of adsorption of glycine onto the surface of $BC_2N$ nanotube, Appl. Surf. Sci. 384 (2016) 230–236.

[53] I. Silaghi-Dumitrescu, F. Lara-Ochoa, I. Haiduc, $A_{12}B_{12}$ (A = B, Al; B = N,P) 4/6 fullerene-like cages and their hydrogenated forms stabilized by exohedral bonds. An AM1 molecular orbital study, J. Mol. Struct. 370 (1996) 17–23.

[54] A. Shokuhi Rad, K. Ayub, Adsorption of pyrrole on $Al_{12}N_{12}$, $Al_{12}P_{12}$, $B_{12}N_{12}$, and $B_{12}P_{12}$ fullerene-like nano-cages; a first principles study, Vacuum 131 (2016) 135–141.

[55] A. Shokuhi Rad, K. Ayub, Adsorption of thiophene on the surfaces of $X_{12}Y_{12}$ (X = Al, B, and Y = N,P) nanoclusters; A DFT study, J. Mol. Liq. 238 (2017) 303–309.

[56] N. Abdolahi, M. Aghaei, A. Soltani, Z. Azmoodeh, H. Balakheyli, F. Heidari, Adsorption of celecoxib on $B_{12}N_{12}$ fullerene: spectroscopic and DFT/TD-DFT study, Spectrochim. Acta A Mol. Biomol. Spectrosc. 204 (2018) 348–353.

[57] T. Oku, A. Nishiwaki, I. Narita, Formation and atomic structure of $B_{12}N_{12}$ nanocage clusters studied by mass spectrometry and cluster calculation, Sci. Technol. Adv. Mater. 5 (2004) 635–638.

[58] T. Oku, M. Kuno, H. Kitahara, I. Narita, Int. J. Inorg. Mater. 3 (2001) 597–612.

[59] F. Li, Y. Zhang, H. Chen, Geometric and electronic structures of $B_{12}C_6N_6$ fullerene, Phys. E 56 (2014) 216–221.

[60] P.K. Chattaraj, U. Sarkar, D.R. Roy, Electrophilicity index. Chem. Rev. 106 (2006) 2065–2091.

[61] M.T. Baei, M. Ramezani Taghartapeh, E. Tazikeh Lemeski, A. Soltani, Computational study of $OCN^-$ chemisorption over AlN nanostructures, Superlattice Microstruct. 72 (2014) 370–382.

[62] E. Lebon, R. Sylvain, R.E. Piau, C. Lanthony, J. Pilme, P. Sutra, M. Boggio-Pasqua, J.-L. Heully, F. Alary, A. Juris, A. Igau, Phosphoryl group as a strong σ-donor anionic phosphine-type ligand: a combined experimental and theoretical study on long lived room temperature luminescence of the [Ru(tpy)(bpy)(Ph2PO)]+ complex, Inorg. Chem. 53 (4) (2014) 1946–1948.

[63] Z. Shariatinia, S. Shahidi, A DFT study on the physical adsorption of cyclophosphamide derivatives on the surface of fullerene $C_{60}$ nanocage, J. Mol. Graph. Model. 52 (2014) 71–81.

[64] M. El Khalifi, E. Duverger, T. Gharbi, H. Boulahdour, F. Picaud, Theoretical use of boron nitride nanotubes as a perfect container for anticancer molecules, Anal. Methods 8 (2016) 1367–1372.

[65] Y. Emre Osmanoglu, A. Tokatlı, K. Sutcu, S. Osmanoglu, F. Ucun, Conformational, IR, NMR, and EPR analysis of IFO by density functional theory calculation, Monatshefte Chem. 148 (2017) 227–236.

[66] L.J. Bellamy, L. Beecher, The infra-red spectra of organo-phosphorus compounds. Part III. Aliphatic acids and compounds related to natural products, J. Chem. Soc. (1953) 728–732.

[67] G.C. Loh, Sandeep Nigam, G. Mallick, Ravindra Pandey, Carbon-doped boron nitride nanomesh: stability and electronic properties of adsorbed hydrogen and oxygen, J. Phys. Chem. C 118 (2014) 23888–23896.

[68] M. Garg, R. Naidu, A. Birhade, K. Iyer, R. Jadhav, J. Rebello, N. Morde, M. Mangale, B. Brashie, Bioequivalence of two formulations of salmeterol xinafoate/fluticasone propionate HFA pMDI in healthy volunteers, J. Bioequivalence Bioavailab. 9 (6) (2017) 536–546.

[69] E. Tazikeh Lemeski, A. Soltani, M.T. Baei, M. Bezi Javan, S. Moazen Rad, Theoretical study on pure and doped $B_{12}N_{12}$ fullerenes as thiophene sensor, Adsorption 24 (2018) 585–593.

[70] E. Vessally, M.D. Esrafili, R. Nurazar, P. Nematollahi, A. Bekhradnia, A DFT study on electronic and optical properties of aspirin-functionalized $B_{12}N_{12}$ fullerene-like nanocluster, Struct. Chem. 28 (2017) 735–748.